JOURNAL OF PROPULSION AND POWER
Vol. 25, No. 4, July–August 2009

# Tip-Clearance Effects on Hot-Streak Migration in Low-Pressure Stage of Vaneless Counter-Rotating Turbine

Qingjun Zhao,* Huishe Wang,† Xiaolu Zhao,‡ and Jianzhong Xu‡
*Chinese Academy of Sciences, Beijing, 100190, China*

DOI: 10.2514/1.39102

**Three-dimensional multiblade row unsteady Navier–Stokes simulations have been performed to reveal the effects of rotor tip clearance on the inlet hot-streak migration characteristics in the low-pressure stage of a vaneless counter-rotating turbine. The numerical results indicate that most of the hotter fluid migrates toward the rotor pressure surface and that only a small amount of hotter fluid migrates to the rotor suction surface when it convects into the low-pressure turbine rotor. The hotter fluid that migrated to the tip region of the high-pressure turbine rotor impinges on the leading edge of the low-pressure turbine rotor after it goes through the high-pressure turbine rotor. The migration of the hotter fluid directly results in a very high heat load at the leading edge of the low-pressure turbine rotor. The leakage flow in the rotor tip clearance tends to increase the low-pressure turbine rotor outlet temperature at the tip region.**

## Nomenclature

| | | |
|---|---|---|
| $a$ | = | velocity of sound |
| $c$ | = | nondimensional chord |
| $P$ | = | static pressure |
| SWR | = | ratio of specific work of the high-pressure turbine to that of the low-pressure turbine |
| $T$ | = | static temperature |
| $u$ | = | $x$ components of velocity |
| $v$ | = | $y$ components of velocity |
| $w$ | = | $z$ components of velocity |
| $V$ | = | absolute velocity |
| $\rho$ | = | density |

*Subscripts*

| | | |
|---|---|---|
| 6 | = | low-pressure rotor exit quantity |
| cr | = | critical value |
| hs | = | hot-streak quantity |
| $x$ | = | axial direction |
| $\infty$ | = | freestream quantity |

*Superscript*

| | | |
|---|---|---|
| $*$ | = | total quantity |

## Introduction

A VANELESS counter-rotating turbine (VCRT) is composed of a highly loaded single-stage high-pressure turbine (HPT) and a single-stage vaneless counter-rotating low-pressure turbine/rotor (LPT/LPR). Because of the parts elimination and size reduction, the VCRT can offer some significant benefits compared with a conventional two-stage turbine, even a $1 + 1$ counter-rotating turbine, such as the elevated thrust-to-weight ratio of the aeroengine, the improved performance of aircraft, the reduced cooling flow, and so on [1–4]. Since the 1950s, counter-rotating turbines have been carefully investigated [1–6]. Besides military engines, the counter-rotating turbine systems (CRTS) will also be selected for airline engines for the aim of economy in the future.

Experimental data taken from gas turbine combustors indicate that the flow exiting the combustor can contain both circumferential and radial temperature gradients. The phenomenon is known as hot streaks. The hot streaks arise from the combination of the combustor core flow with the combustor bypass and combustor surface cooling flows. In a turbine, the hot streaks convect through the vanes and interact with the rotor blades. They can cause local hot spots on the blade surfaces, leading to heat fatigue of the blade and reducing the blade's life. Through the investigation on inlet hot-streak migration, the unsteady temperature field on the blade surfaces can be identified. This information is beneficial to the blade cooling design, prolonging the blade's life and increasing the turbine's efficiency.

Earlier research on streamline pattern showed theoretically that inflow temperature gradients will not alter the streamline pattern in vanes as long as the inflow total pressure is uniform [7]. However, subsequent research on the secondary flow of a rotating system, which was performed by Lakshminarayana and Horlock [8], indicated that inflow temperature nonuniformities can lead to a secondary flow in the rotating blade rows. Butler et al. [9] carried out an experimental investigation of hot-streak migration using a large-scale rotating rig (LSRR). They also found that the temperature gradients did not alter the flow within the turbine stator, but had a significant impact on the flowfield of the rotor blade rows when the total pressure in the distortion was uniform. Their conclusion has been verified by some other experimental and numerical investigations [10,11]. The results, which were obtained by Butler et al. [9], Roback and Dring [10], and Sharma et al. [12] through experimental and numerical investigations, showed that hot streaks cause hotter gas to accumulate on the rotor blade pressure surfaces (PS) and colder gas to accumulate on the rotor blade suction surfaces. However, the numerical investigation results of Gundy-Burlet and Dorney [13] indicated that the migration patterns of hot streaks are directly related to the position of the hot streak in relation to the first-stage stator. When the hot streak impinges the leading edge (LE) of the first-stage stator, the hot gases are convected with the stator wake and migrate to the suction surface (SS) of the first-stage rotor. On the contrary, the hot gases migrate to the pressure surface of the first-stage rotor when the hot streak is located in the midpitch of the first-stage stator vanes. The different characteristics of hot-streak migration in rotor blade rows should be investigated in detail. In addition to the secondary flow and circumferentially relative location

Received 13 June 2008; revision received 5 March 2009; accepted for publication 15 April 2009. 

*Assistant Professor, Institute of Engineering Thermophysics, Post Office Box 2706.
†Associate Professor, Institute of Engineering Thermophysics, Post Office Box 2706.
‡Professor, Institute of Engineering Thermophysics, Post Office Box 2706.

effect, Shang and Epstein [14] showed that hot-streak migration is also affected by buoyancy, which tends to drive the hot streak toward the hub. Gundy-Burlet and Dorney [15] investigated the effects of radial location on the migration of hot streaks in a turbine. Through this investigation, they think hot streak impinged directly on the first-stage stator and located in the lower half-span of the airfoil passage suggest should be introduced. Orkwis et al. [16] and Sondak et al. [17] performed some simulations on hot-streak effects using a new linear Navier–Stokes solver. The results indicated that the linear technique is a valuable tool for including the effects of hot-streak unsteadiness in design analyses. Sondak et al. [17] also carried out hot-streak clocking simulations using nonlinear and linearized Navier–Stokes solvers for two blade-count configurations. The results show that the linearized technique can be used to qualitatively predict hot-streak clocking effects. The results also indicated that the reduced-blade-count approximation has a significant impact on predicted surface temperatures. The effects of blade count were also investigated by Shang and Epstein [14]. They found that the heat load on rotor blades can be reduced by the selection of the nozzle guide vane (NGV)/rotor blade count ratio. He et al. [18] explored the effects of the circumferential wavelength of a hot streak. Their results indicated that the circumferential wavelength of the hot streak can significantly change the unsteady forcing and the heat load on rotor blades.

The experimental facilities most often used in hot-streak investigations include the LSRR [9,10], the warm core turbine test rig (WCTTR) [19], and the blowdown turbine test rig (BTTR) [20]. The LSRR experiments were performed at low speed, but the blade surface temperature ($CO_2$ concentrations) was measured. In the WCTTR experiments, the blade surface temperature was not measured, but it is a high-speed rig. Compared with LSRR and WCTTR, the BTTR experiments were not only performed at high speed, but the blade surface temperature was also measured. Shang et al. [21] performed hot-streak experiments using BTTR to examine the effects of hot-streak migration on the blade surface temperature at a high speed.

Harasgama [22] performed a numerical simulation of radial temperature distortion at the inlet to a rotating turbine rotor. The results show that the hot gas is transported to the pressure surface of the blade and that hot gas also migrates to the blade pressure side tip. At locations greater than 50–60% axial chord, the hot gas enters the tip gap and emerges over the suction side. The results also indicate that the secondary flows within the turbine rotor are enhanced by the introduction of inlet radial temperature distortion. The heat flux near the tip region on the pressure side of the blade can be increased by up to 76% due to the redistribution of the inlet temperature distortion. The numerical investigations preformed by Gundy-Burlet [23] show that the hot streak directly impinging on the leading edge of the first-stage stator results in low levels of heat transfer on the second-stage stator. And the results illustrate that relatively high heat transfer on the first-stage rotor is localized to the leading edge, hub vortex, and tip leakage flow regions. Castillon et al. [24] carried out an unsteady three-dimensional numerical analysis on a hot-streak transport through an axial high-pressure turbine stage. The predicted results confirm the conclusion: if the hot streak is located in front of the NGV leading edge, the rotor blade experiences significant heat transfer reduction compared with an inlet midpassage location. And the reattachment lines rooted in the tip leakage vortex were observed around 90% span of the rotor. The results also show that the hot gas driven on the pressure surface of the rotor can convect into the tip gap and migrate to the suction surface.

In this paper, the effects of tip clearance on the hot-streak migration in the low-pressure stage of the VCRT will be explored by means of three-dimensional unsteady numerical simulations.

## Numerical Algorithm

NUMECA's software systems are employed to study this problem. The numerical method is described in detail in the user manual [25]. Here, only a brief description of the main features is reported.

The governing equations in NUMECA are the time-dependent, three-dimensional Reynolds-averaged Navier–Stokes equations. The solver of NUMECA is FINE/Turbo, and it is based on a cell-centered finite volume approach, associated with a central space discretization scheme together with an explicit four-stage Runge–Kutta time integration method.

Residual smoothing, local time-stepping, and multigridding are employed to speed up convergence to the steady-state solution. The dual time-stepping method [26] and domain-scaling method [27] are used to perform time-accurate calculations.

Various turbulence models have been included in the solver for the closure of governing equations. The widely used approach based on Spalart–Allmaras's one transport equation [28] has been selected in this paper.

## Boundary Conditions

The theory of characteristics is used to determine the boundary conditions at the inlet and exit of the computational domain. The total temperature is specified as a function of the spatial coordinates at the inlet. The total pressure and the circumferential and radial flow angles are given as constants at the inlet.

In these simulations, the flow variables in the hot streak must be modified. In the hot streak, the inlet flow variables used to define the specified boundary conditions can be written as

$$
\begin{aligned}
u_{\mathrm{hs}} &= u_\infty \sqrt{T_{\mathrm{hs}}/T_\infty} \qquad & v_{\mathrm{hs}} &= v_\infty \sqrt{T_{\mathrm{hs}}/T_\infty} \\
w_{\mathrm{hs}} &= w_\infty \sqrt{T_{\mathrm{hs}}/T_\infty} \qquad & P_{\mathrm{hs}} &= P_\infty \\
a_{\mathrm{hs}} &= a_\infty \sqrt{T_{\mathrm{hs}}/T_\infty} \qquad & \rho_{\mathrm{hs}} &= \rho_\infty/(T_{\mathrm{hs}}/T_\infty)
\end{aligned} \tag{1}
$$

where $T_{\mathrm{hs}}$ is the static temperature within the hot streak, and $T_\infty$ is the static temperature of the unaffected inlet flow. The static and total pressures within the hot streak are assumed to be equal to that of the unaffected inlet flow.

At the exit, the circumferential and radial velocity components, the entropy, and the downstream running Riemann invariant are extrapolated from the interior of the computational domain. The static pressure, $P_6$, is specified at the hub of the exit, and the static pressure values at all other radial locations are obtained by integrating the equation for radial equilibrium. Periodicity is enforced along the outer boundaries of the H–O–H grids in the circumferential direction.

In this paper, absolute no-slip boundary conditions are enforced at the hub and tip end walls of the HPT stator regions, along the surface of the HPT vane, and along the casing walls of the HPT rotor and LPR regions. Relative no-slip boundary conditions are imposed at the hub end walls of the HPT rotor and LPR regions and the surfaces of the HPT rotor and LPR blades. It is assumed that the normal derivative of pressure is zero at the solid wall surfaces and that the walls are adiabatic.

## Vaneless Counter-Rotating Turbine

The VCRT studied in this paper is composed of a highly loaded single-stage HPT coupled with a vaneless counter-rotating LPT/LPR. It has high expansion ratio and operates in transonic regimes. The VCRT has some unique characteristics, which are different from the conventional two-stage turbine, even a $1 + 1$ counter-rotating turbine. These characteristics are as follows: 1) the HPT rotor and LPT/LPR are counter-rotating, 2) the LPT is vaneless, and 3) there is a high relative Mach number ($\sim$1.5) and relative flow angle ($\sim$70°) at the outlet of the HPT. The design conditions of the VCRT are shown in Table 1.

The airfoil counts in the steady and unsteady model are reduced from the actual count of 36/36/36 for the HPT stator, HPT rotor, and LPR, respectively, to 1/1/1 for computational efficiency. The tip clearance size studied in this paper is 2.0 mm (2.59% HPT rotor height and 2.09% LPR height) (see Fig. 1). The typical $y^+$ values of less than 15 are used at the boundaries. All of these determine computational fluid dynamics models with about 0.42 (without tip

**Table 1 Flow conditions in the VCRT**

| | |
|---|---|
| Inlet total temperature, K | 500 |
| Inlet total pressure, kPa | 300 |
| Mass flow, kg/s | 17.7 |
| Rotational speed of HPT rotor, rpm | 6970 |
| Rotational speed of LPR, rpm | −6970 |
| Expansion ratio of HPT | 2.93 |
| Expansion ratio of LPT | 2.07 |
| SWR | 1.77 |

clearance case 1) and 0.57 (with tip clearance case 2) million grid points employing a sheared H–O–H mesh generated by NUMECA's AutoGrid (see Fig. 2). It will take about one week to compute an unsteady case using one 3.0 GHz Intel CPU computer. According to past experiences, which were obtained in the unsteady three-dimensional viscous analyses about the VCRT [3], the grid size selected in this paper is adequate to the investigation.

## Validating the Numerical Code

To validate the predicted accuracy of the numerical code, a three-dimensional multistage unsteady Navier–Stokes simulation with an inlet radial hot streak has been performed in a test turbine. Then, the time-averaged numerical data are compared with the available experimental data. The test turbine is a 0.767-scale rig modeling the first stage of a two-stage core turbine designed for a modern high-bypass-ratio engine. The vane has a constant section and was designed for a constant exit flow angle of 75 deg from the axial direction. The rotor inlet was designed to accept the vane exit flow with either zero or a slight negative incidence. The rotor outlet is a free-vortex design. Both vane and blade axial chords are constant radially. The experimental turbine has 26 vane airfoils and 48 rotor airfoils. It was tested in the WCTTR [19,29]. The test conditions for the turbine are shown in Table 2.

The inlet radial temperature profile in the experiment was produced using the combustor exit radial temperature simulator (CERTS) inlet, which injected cool air through circumferential slots in the hub and tip end walls upstream of the vane. Figure 3 shows the circumferentially averaged temperature distribution at the turbine inlet. The ratio of the maximum total temperature to the average total temperature is approximately 1.05, and the ratio of the maximum to the minimum total temperature is approximately 1.20 at the turbine inlet.

To reduce the cost of the calculation, the number of vanes in the first row is decreased to 24 and the size of the vane is increased by a factor of 26/24 to maintain the same blockage. Thus, a one-vane/two-rotor airfoil count ratio is used in the unsteady numerical simulation. And two geometry configurations, one with a 1.2% tip clearance and one without tip clearance for the rotor, are selected in the numerical simulations.

Figures 4–6 show a comparison between the predicted and experimental time-averaged critical velocity ratio distributions at the hub, midspan, and tip of the vane, individually. The predicted data are very close to the experimental data, except for the suction surface near the trailing-edge region at the hub of the vane, near the 40% axial chord region at the midspan, and the tip of the vane. The discrepancy between the computational and the experimental results is basically attributed to the application of the domain-scaling method in the numerical simulation.

Figure 7 illustrates the predicted and experimental total pressure distributions at the outlet of the turbine. There is good agreement between the predicted and experimental results. Compared with the experimental results, the predicted accuracy of the case with a 1.2% rotor tip clearance is higher than the case without rotor tip clearance at the tip region of the turbine outlet. The reason is that the geometry configuration of the case with a 1.2% rotor tip clearance is the same as that of the experiment. The tip clearance effects are considered for the case with a 1.2% rotor tip clearance.

Figure 8 shows the predicted and experimental total temperature distributions at the outlet of the turbine. The predicted values show close agreement with the experimental values from the hub to 70% span. Although the discrepancies between the numerical and experimental data are apparent from 70% span to the tip, the trends predicting total temperature distributions are similar to the experimental trends. And because the tip clearance effects were considered, the results of the case with a 1.2% rotor tip clearance are closer to the experimental results than those of the case without tip clearance.

The aforementioned results indicate that the flow characteristics in the high subsonic turbine can be qualitatively predicted by means of the numerical code. The numerical code is acceptable in this investigation.

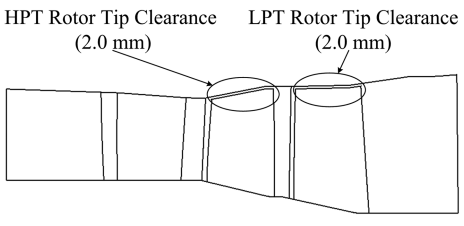


**Fig. 1 Meridional section of the VCRT with rotor tip gap.**

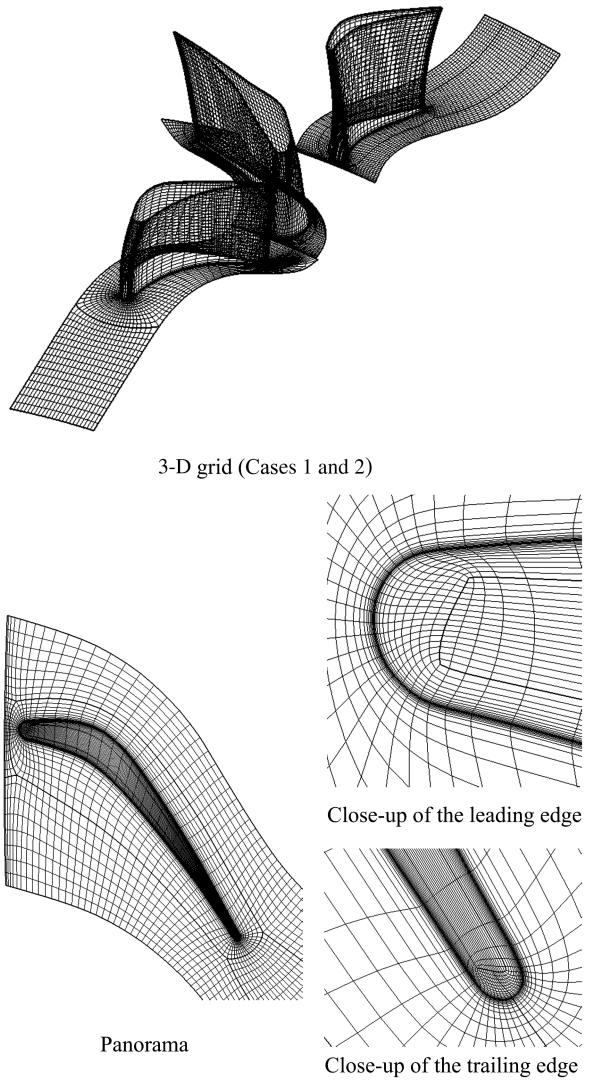


**Fig. 2 H–O–H grid topologies of the VCRT.**

**Table 2 Flow conditions in the test turbine**

| | |
|---|---|
| Inlet total temperature, K | 672.2 |
| Inlet total pressure, Pa | $3.103 \times 10^5$ |
| Mass flow, kg/s | 6.13 |
| Specific work, J/kg | $1.299 \times 10^5$ |
| Rotational speed, rpm | 11373 |
| Total pressure ratio | 2.36 |
| Load factor | 1.675 |
| Flow coefficient | 0.449 |

## Inlet Hot-Streak Profile

In this paper, a hot-streak temperature ratio of 2.0 measured at the outlet of a typical short annular combustion chamber is selected. The hot streak is circular in shape with a diameter equal to 25% of the HPT stator span. The hot-streak center is located at 50% of the span and the leading edge of the HPT stator. The hot-streak profile is shown in Fig. 9.

## Numerical Results

Figure 10 shows the instantaneous Mach number contours on the midspan section of the HPT rotor for the case with rotor tip clearance. There are two high-strength shock waves originating from the trailing edge of the HPT rotor, which are called the inner-extending shock wave (IESW) and outer-extending shock wave (OESW), respectively. And a series of compression waves emanates from the rotor suction surface at about 64–82% axial chord region. The interaction between these compression waves and the IESW can be observed in the HPT rotor. Figure 10 shows that the wave system is very complex in the HPT rotor. The peak Mach number is approximately 2.0 in the HPT rotor. Such a high Mach number is unusual in a transonic turbine rotor. The complicated wave system and high outlet Mach number result in some unique aerodynamic characteristics in the HPT rotor compared with a conventional two-stage turbine. And these waves can also affect the migration of the hot-streak fluid in the HPT rotor. Because of a weak effect of leakage flow on the midspan fluid of the HPT rotor and the LPR, the wave system on the midspan section in case 1 is very similar to case 2.

Figure 11 shows the static temperature contour on the midspan of the HPT rotor and LPR at one instant in time for case 1. The secondary flow and buoyancy cause the temperature redistribution in the HPT rotor when the hot streak mixes with the HPT vane wake and flows into the HPT rotor. Most of the hotter fluid convects toward the pressure surface of the HPT rotor, whereas most of the colder fluid

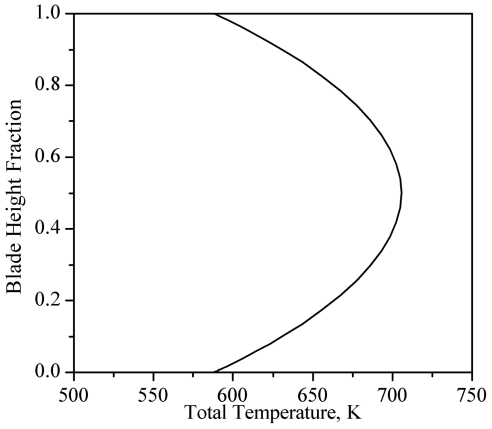


**Fig. 3 Turbine inlet radial temperature profile.**

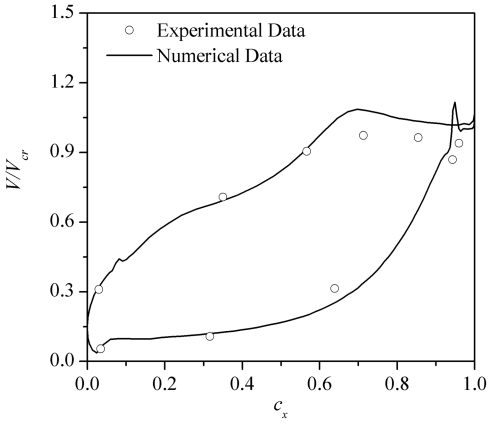


**Fig. 4 Critical velocity ratio at the hub of the vane.**

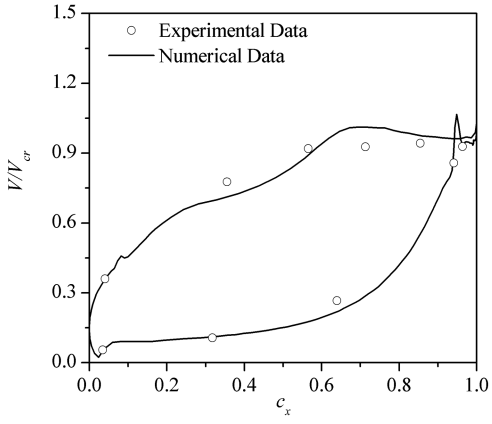


**Fig. 5 Critical velocity ratio at the midspan of the vane.**

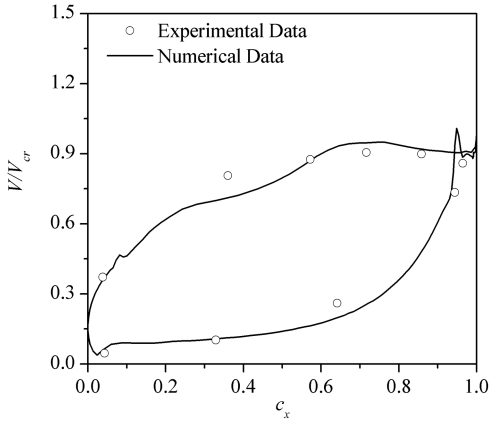


**Fig. 6 Critical velocity ratio at the tip of the vane.**

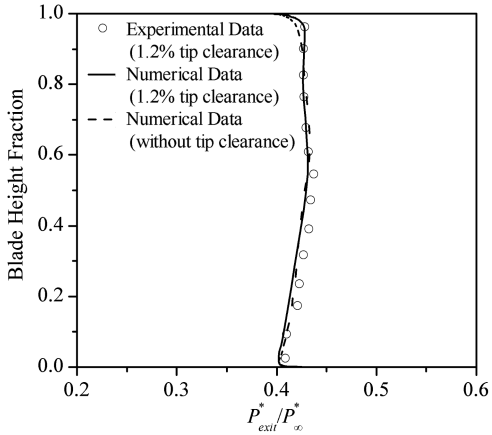


**Fig. 7 Total pressure distribution at the outlet of the turbine.**

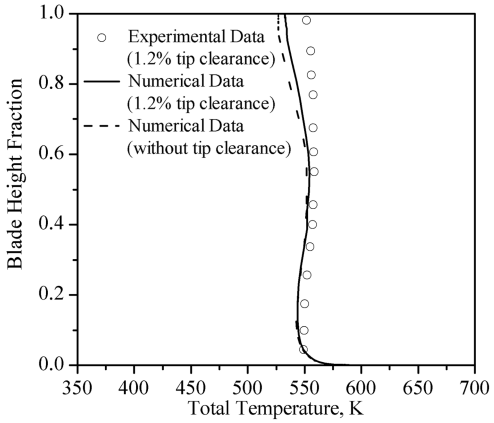


**Fig. 8 Total temperature distribution at the outlet of the turbine.**

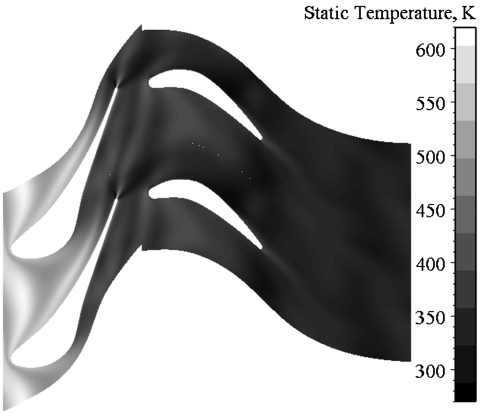


**Fig. 11 Instantaneous static temperature contour on the midspan section of the HPT rotor and LPR: case 1.**

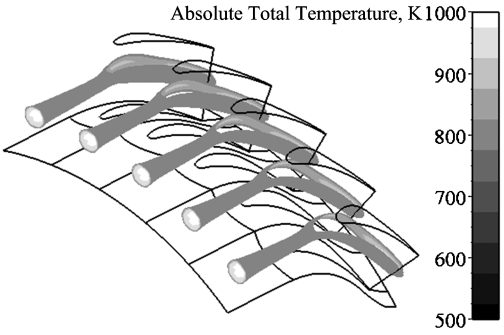


**Fig. 9 Inlet hot-streak profile (cases 1 and 2).**

migrates to the suction surface of the HPT rotor. And some hotter fluid also rounds the leading edge of the HPT rotor and migrates to the suction surface of the rotor. The hotter fluid, which has migrated to the pressure surface of the HPT rotor, goes through the HPT rotor along the pressure surface. It penetrates through the IESW at the trailing edge of the HPT rotor and encounters the OESW at the interface between the HPT rotor and the LPR. Then it mixes with the wake of the HPT rotor. And the OESW also has an effect on the mixed fluid. Finally, the mixed fluid is cut by the LPR and convects toward the pressure surface of the LPR. On the other hand, most of the colder fluid that has migrated to the suction surface of the HPT rotor goes through the HPT rotor along the suction surface. It penetrates through the IESW at about 60% axial chord of the HPT rotor and pierces the OESW at the trailing edge of the HPT rotor. After interacting with the OESW, it is cut by the LPR and migrates to the suction surface of the LPR. Because of a weak effect of leakage flow on the midspan fluid of the HPT rotor and the LPR, the temperature distribution on the midspan section in case 2 is very similar to case 1.

Figure 12 describes the leakage flow in the LPR blade tip clearance. The fluid near the pressure surface tip region can be driven to the rotor suction surface by the leakage flow. In the LPR, some of the hotter fluid that migrated to the pressure surface tip region will convect into the suction side of the rotor. The migration induced by the leakage flow directly results in an intensified heat load on the rotor suction surface. Figure 13 more clearly illustrates the aforementioned phenomenon. Figure 13 also shows that the gas temperature near the casing wall is higher than the hot-streak center temperature in the LPR. The tip high-temperature region is directly related to the leakage flow in the HPT rotor. In the HPT rotor, some of the high-temperature gas that migrated into the tip clearance will go

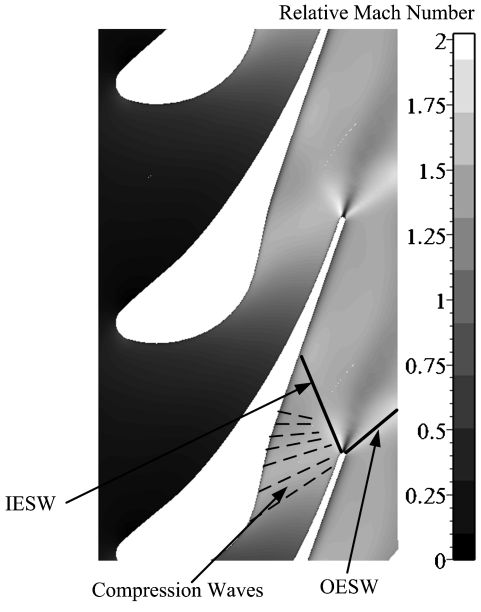


**Fig. 10 Instantaneous Mach number contours on the midspan section of the HPT rotor.**

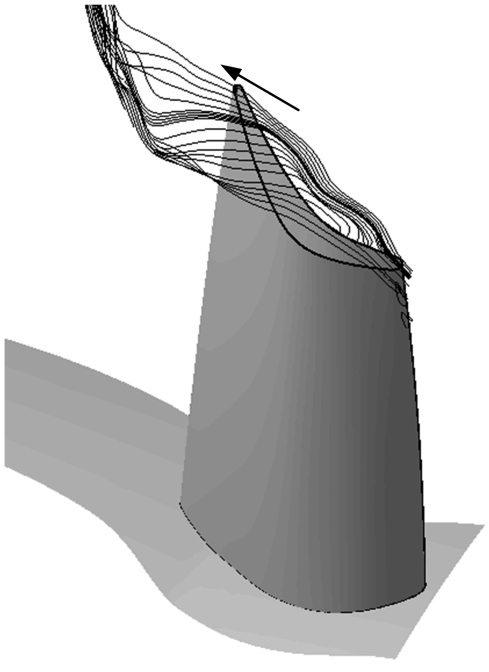

**Fig. 12 LPR blade tip leakage flow.**

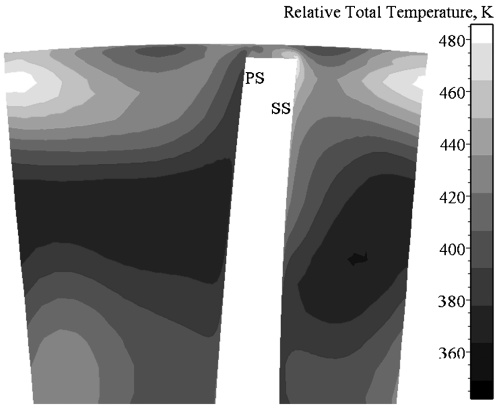


**Fig. 13 Instantaneous temperature contour on a cross section (S3 section) of the LPR passage: case 2.**

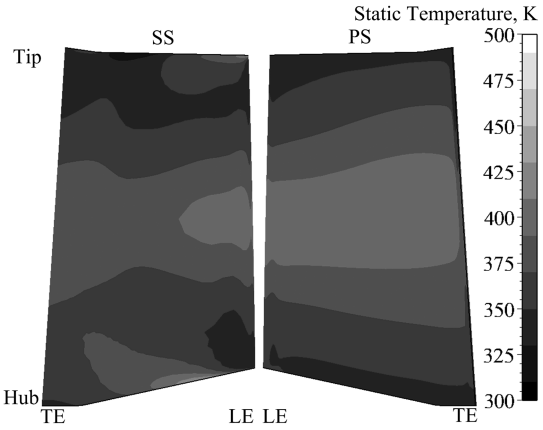


**Fig. 16 Time-averaged static temperature contour on the LPR: case 1.**

through the HPT rotor along the gap and convect into the LPR. The migration of the high-temperature gas induces the extreme high-temperature region at the tip region of the LPR.

The instantaneous temperature distributions at the LPR inlet for cases 1 and 2 are shown in Figs. 14 and 15. Comparing the results in Figs. 14 and 15, it is well know that the leakage flow in the HPT rotor tends to increase the LPR inlet temperature at the tip region. The phenomenon is consistent with Fig. 13. The highest temperature region shown in Fig. 15 is ascribed the effect of tip leakage flow on the hot-streak fluid in the HPT rotor. The tip leakage flow drives the hot-streak fluid into the tip clearance in the HPT rotor. Then, the hot-streak fluid is migrated toward the downstream of the HPT rotor along the tip region. Finally, the hot-streak fluid convects into the LPR and impinges on the leading edge of the LPR. This migration results in the increase in the temperature at the tip region of the LPR leading edge. The air flow with a higher temperature at the tip region of the LPR inlet will affect the flow and heat transfer characteristics in the LPT.

Figure 16 shows the time-averaged static temperature contour on the LPR for case 1 (without tip clearance). There are two regions with an elevated adiabatic wall temperature on the suction surface. The larger high-temperature region originates from the hub at about 15% axial chord and extends radially toward the trailing edge. The second high-temperature region emanates from the tip at the leading edge and extends inverse radially to the 50% axial chord at about 88% span. These two high-temperature regions are directly associated with the secondary flow in the LPR. The result has been proved in [4], along with a more detailed description of the effects of the secondary flow. In addition to the influence of the secondary flow, the shock wave in the LPR also effects the high-temperature region that emanates from the hub. The time-averaged relative Mach number distributions on the hub section of the LPR for case 1 are shown in Fig. 17. The temperature distributions on the hub region of the LPR suction surface are affected by the shock wave originating from the suction surface. In the LPR, the high-temperature region originating from the hub is directly related to the interaction between the secondary flow and the shock wave. Figure 16 indicates that there is still a larger high-temperature region on the suction surface of the LPR besides the aforementioned two high-temperature regions. The high-temperature region is directly induced by the inlet hot streak. The region emanates from the leading edge and extends axially toward the trailing edge. The radial extent of this region decreases as it approaches the trailing edge due to the effect of the secondary flow. Figure 16 also shows that there is a larger high-temperature region on the pressure surface of the LPR, which is associated with the inlet hot steak. The region originates from the leading edge and extends axially toward the trailing edge. The radial extent of this region increases as it approaches the trailing edge due to the influence of the

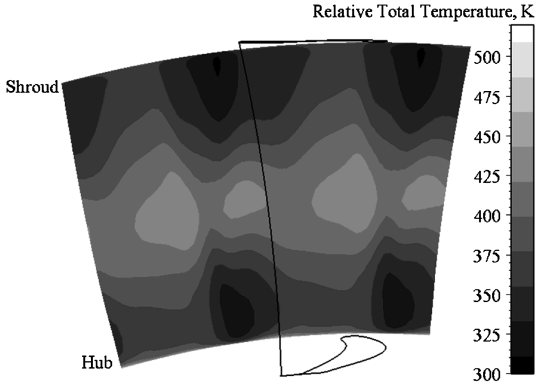


**Fig. 14 Instantaneous temperature contour at the LPR inlet: case 1.**

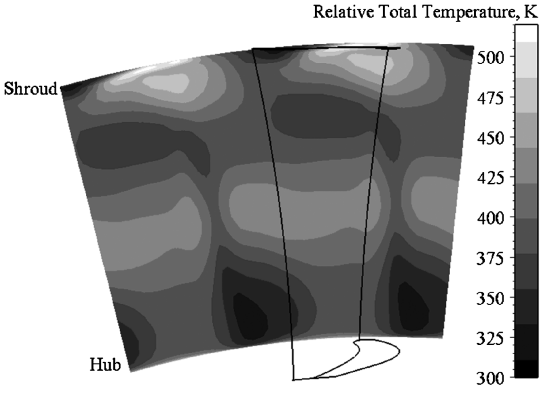


**Fig. 15 Instantaneous temperature contour at the LPR inlet: case 2.**

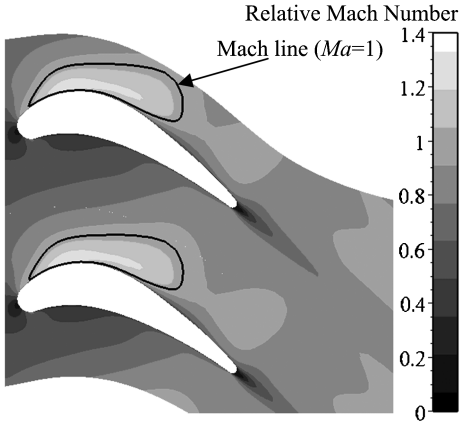


**Fig. 17 Time-averaged Mach number contour on the hub section of the LPR: case 1.**

secondary flow. The temperature distribution on the LPR surface indicates that most of the hot-streak fluid migrates toward the pressure surface as it convects into the LPR. The migrating characteristics of the hot-streak fluid are dominated by the secondary flow in the LPR. The effect of the buoyancy on the high-temperature fluid near the LPR blade surface is very weak. On the pressure surface of the LPR, the secondary flow drives the hotter fluid toward the hub and tip, whereas, on the suction surface of the LPR, the secondary flow makes the hotter fluid migrate toward the midspan.

Figure 18 shows the time-averaged static temperature contour on the LPR for case 2 (with tip clearance). There are three regions with elevated adiabatic wall temperature on the suction surface of the LPR. The first high-temperature region related to the interaction between the secondary flow and the shock wave originates from the hub at about 15% axial chord and extends radially to the trailing edge at about 25% span. The second high-temperature region associated with the combined effects of secondary and tip leakage flows emanates from the tip at the leading edge and extends inverse radially to the trailing edge at about 65% span. The third high-temperature region related to the inlet hot streak emanates from the leading edge and extends axially toward the trailing edge. The radial extent of this region decreases approaching the trailing edge due to the effect of the secondary flow. On the suction surface of the LPR, the secondary flow drives the hot-streak fluid toward the midspan. On the other hand, the tip leakage flow also has an effect on the hot-streak fluid that migrated to the suction surface of the LPR. The tip leakage flow induces the hot-streak fluid to migrate toward the hub on the suction surface of the LPR. It is well known that the temperature of the second high-temperature region is highest compared with the other two high-temperature regions. The reason is that the leakage flow in the HPT rotor directly drives hotter fluid toward the tip region of the LPR. Then the secondary flow and leakage flow will drive the hotter fluid to the trailing edge of the LPR along the inverse radial and axial directions. The migration of the hotter gas induces the extreme high-temperature region at the tip region of the LPR. Figure 18 also shows that there is a larger high-temperature region on the pressure surface of the LPR, which is related to the inlet hot steak. The region originates from the leading edge and extends axially toward the trailing edge. The radial extent of this region increases as it approaches the trailing edge due to the influence of the secondary and tip leakage flows. On the pressure surface of the LPR, the secondary flow drives the hotter fluid toward the hub and tip, and the leakage flow drives the hotter fluid toward the tip. The migration of the hotter fluid on the pressure surface directly induces the high-temperature region. The temperature distribution on the LPR surface also indicates that most of the hot-streak fluid migrates toward the pressure surface as it convects into the LPR. The migrating characteristics of the hot-streak fluid are dominated by the combined effects of the secondary and tip leakage flows in the LPR.

It is well known that the heat load of the LPR is intensified due to the effects of the tip leakage flow, as seen in a comparison of Figs. 16 and 18.

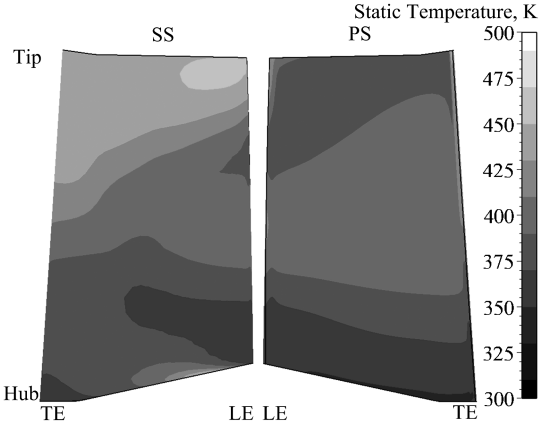


**Fig. 18 Time-averaged static temperature contour on the LPR: case 2.**

Figure 19 indicates the time-averaged relative total temperature distributions in the LPR passages for cases 1 and 2. In these two cases, the secondary flow drives the hot-streak fluid toward the pressure surface along the flow direction. When the hot-streak fluid migrates to the pressure surface, the secondary flow will drive it toward the hub and tip along the flow direction. And the secondary flow also drives the colder fluid toward the suction surface along the flow direction, companying the hot steak fluid movements. As the colder fluid migrates to the suction surface, the secondary flow drives the colder fluid toward the midspan along the flow direction. A small amount of the hot-streak fluid, which rounds the leading edge of the LPR and migrates to the suction surface, also moves toward the midspan along the flow direction under the effect of the secondary flow. Comparing the results of cases 1 and 2 in Fig. 19, it is well known that the radial migration of the hot-streak fluid is also dominated by the leakage flow in the rotor tip clearance. The leakage flow tends to drive the hotter fluid toward the blade tip on the pressure surface and to the hub on the suction surface. Figure 19 also indicates that the hotter fluid that migrated to the tip region at the leading edge of the LPR through the tip clearance of the HPT rotor moves across the tip gap of the LPR and reaches the suction surface. Then the secondary flow and leakage flow will drive the hotter fluid to the trailing edge of the LPR along the inverse radial and axial directions. The migration of the hotter gas directly induces the extreme high-temperature region at the tip region of the LPR. Figure 20 more clearly shows the effects of the tip leakage flow on the hotter fluid. Figure 19 also shows that the leakage flow effect tends to increase the LPR outlet temperature at the tip region. In a word, the existence of

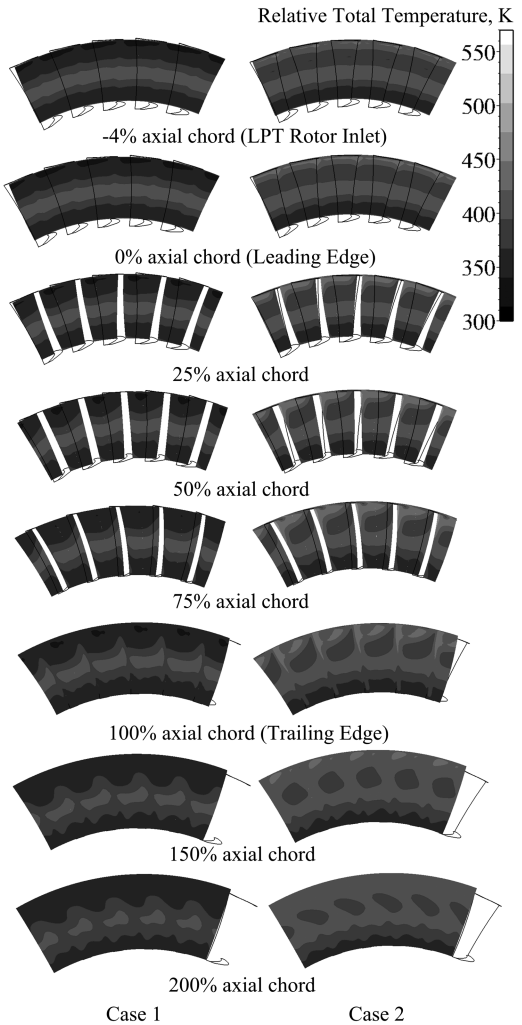


**Fig. 19 Time-averaged relative total temperature contours on some S3 sections of the LPR passage.**

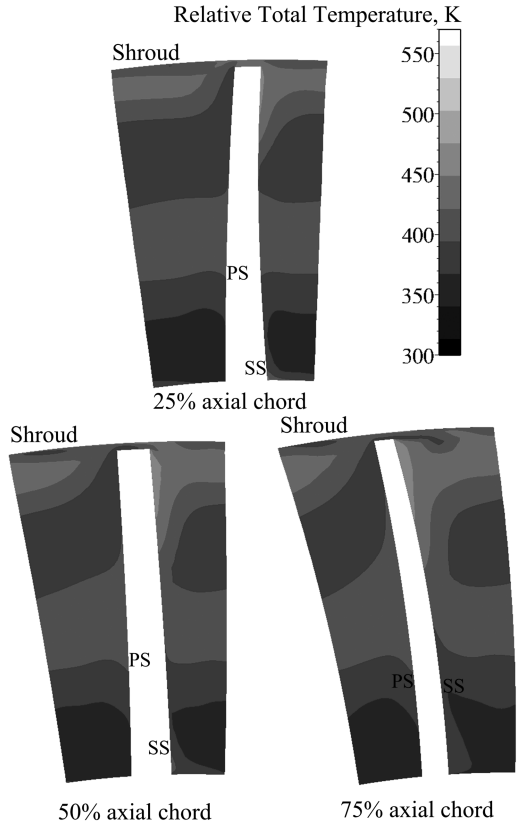


**Fig. 20 Time-averaged relative total temperature contours on three S3 sections of the LPR passage: case 2.**

the tip leakage flow directly results in a different temperature distribution in LPR between cases 1 and 2.

## Conclusions

In this paper, the hot-streak simulation has been performed on a vaneless counter-rotating turbine that is different from a conventional two-stage turbine. Two turbine configurations with and without rotor tip clearance are investigated by a three-dimensional unsteady Navier–Stokes code. Through a comparison of these two different configurations, the effects of rotor tip clearance on the hot-streak migration are specially analyzed in a low-pressure turbine. Based on this numerical investigation, the following conclusions have been drawn:

1) When the hot-streak fluid convects into the low-pressure turbine rotor, its migration direction is determined by the separation effect of the colder and hotter fluid. The separation effect causes most of the hot-streak fluid to migrate toward the rotor pressure surface. This migration increases the temperature of the rotor pressure surface.

2) The hot-streak fluid that migrated from the tip clearance of the high-pressure turbine rotor directly impinges on the leading edge of the low-pressure rotor. This migration is unique in a vaneless counter-rotating turbine. The rotor leading edge undergoes a higher heat load due to the impinging of the hot-streak fluid. The secondary and tip leakage flows drive the hot-streak fluid that impinged the rotor leading edge toward the trailing edge along the inverse radial and axial directions in the low-pressure rotor. The combined effects of secondary and tip leakage flow induces the highest temperature region on the suction surface of the low-pressure rotor. This migration of the hot-streak fluid intensifies the heat load of the tip region on the rotor suction surface.

3) In a vaneless counter-rotating turbine, the hot-streak migration induced by tip leakage flow not only increases the heat load of the whole low-pressure rotor blade, but also enhances the temperature of the tip region at the turbine outlet.

Based on these conclusions, the design of a cooling configuration should focus on these regions influenced by tip leakage flow in low-pressure rotor of a vaneless counter-rotating turbine.

## References

[1] Keith, B. D., Basu, D. K., and Stevens, C., "Aerodynamic Test Results of Controlled Pressure Ratio Engine (COPE) Dual Spool Air Turbine Rotating Rig," American Society of Mechanical Engineers Paper 2000-GT-0632, 2000.

[2] Haldeman, C. W., Dunn, M. G., Abhari, R. S., Johnson, P. D., and Montesdeoca, X. A., "Experimental and Computational Investigation of the Time-Averaged and Time-Resolved Pressure Loading on a Vaneless Counter-Rotating Turbine," American Society of Mechanical Engineers Paper 2000-GT-0445, 2000.

[3] Zhao, Q. J., Wang, H. S., Zhao, X. L., and Xu, J. Z., "Numerical Analysis of 3-D Unsteady Flow in a Vaneless Counter-Rotating Turbine," *Frontiers of Energy and Power Engineering in China*, Vol. 1, No. 3, 2007, pp. 352–358. doi:10.1007/s11708-007-0053-3

[4] Zhao, Q. J., Tang, F., Wang, H. S., Du, J. Y., Zhao, X. L., and Xu, J. Z., "Influence of Hot Streak Temperature Ratio on Low Pressure Stage of a Vaneless Counter-Rotating Turbine," *Journal of Engineering for Gas Turbines and Power*, Vol. 130, No. 3, 2008, pp. 031901-1–031901-10. doi:10.1115/1.2836615

[5] Wintucky, W. T., and Stewart, W. L., "Analysis of Two-Stage Counter-Rotating Turbine Efficiencies in Terms of Work and Speed Requirements," NACA RM-E57L05, 1958.

[6] Louis, J. F., "Axial Flow Contra-Rotating Turbines," American Society of Mechanical Engineers Paper 85-GT-218, 1985.

[7] Munk, M., and Prim, R. C., "On the Multiplicity of Steady Gas Flows Having the Same Streamline Pattern," *Proceedings of the National Academy of Sciences of the United States of America. Physical sciences.*, Vol. 33, 1947, pp. 137–141. doi:10.1073/pnas.33.5.137

[8] Lakshminarayana, B., and Horlock, J. H., "Generalized Expressions for Secondary Vorticity Using Intrinsic Coordinates," *Journal of Fluid Mechanics*, Vol. 59, No. 1, 1973, pp. 97–115. doi:10.1017/S0022112073001448

[9] Butler, T. L., Sharma, O. P., Joslyn, H. D., and Dring, R. P., "Redistribution of an Inlet Temperature Distortion in an Axial Flow Turbine Stage," *Journal of Propulsion and Power*, Vol. 5, No. 1, 1989, pp. 64–71. doi:10.2514/3.23116

[10] Roback, R. J., and Dring, R. P., "Hot Streaks and Phantom Cooling in a Turbine Rotor Passage: Part 1—Separate Effects," *Journal of Turbomachinery*, Vol. 115, No. 4, 1993, pp. 657–666. doi:10.1115/1.2929300

[11] Dorney, D. J., "Numerical Investigation of Hot Streak Temperature Ratio Scaling Effects," AIAA Paper 96-0619, 1996.

[12] Sharma, O. P., Pichett, G. F., and Ni, R. H., "Assessment of Unsteady Flows in Turbines," *Journal of Turbomachinery*, Vol. 114, No. 1, 1992, pp. 79–90. doi:10.1115/1.2928001

[13] Gundy-Burlet, K. L., and Dorney, D. J., "Three-Dimensional Simulations of Hot Streak Clocking in a $1-1/2$ Stage Turbine," AIAA Paper 96-2791, 1996.

[14] Shang, T., and Epstein, A. H., "Analysis of Hot Streak Effects on Turbine Rotor Heat Load," *Journal of Turbomachinery*, Vol. 119, No. 3, 1997, pp. 544–553.

[15] Gundy-Burlet, K. L., and Dorney, D. J., "Effects of Radial Location on the Migration of Hot Streaks in a Turbine," *Journal of Propulsion and Power*, Vol. 16, No. 3, 2000, pp. 377–387. doi:10.2514/2.5589

[16] Orkwis, P. D., Turner, M. G., and Barter, J. W., "Linear Deterministic Source Terms for Hot Streak Simulations," *Journal of Propulsion and Power*, Vol. 18, No. 2, 2002, pp. 383–389. doi:10.2514/2.5946

[17] Sondak, D. L., Gupta, V., Orkwis, P. D., and Dorney, D. J., "Effects of Blade Count on Linearized and Nonlinear Hot Streak Clocking Simulations," *Journal of Propulsion and Power*, Vol. 18, No. 6, 2002, pp. 1273–1279. doi:10.2514/2.6063

[18] He, L., Menshikova, V., and Haller, B. R., "Effect of Hot-Streak Counts on Turbine Blade Heat Load and Forcing," *Journal of Propulsion and Power*, Vol. 23, No. 6, 2007, pp. 1235–1241. doi:10.2514/1.29603

[19] Stabe, R. G., Whitney, W. J., and Moffitt, T. P., "Performance of a High-

Work Low-Aspect Ratio Turbine Tested with a Realistic Inlet Radial Temperature Profile," AIAA Paper 84-1161, 1984.
[20] Guenette, G. R., "A Fully Scaled Short Duration Turbine Experiment," Sc.D. Dissertation, Aeronautics and Astronautics Dept., Massachusetts Inst. of Technology, Cambridge, MA, 1985.
[21] Shang, T., Guenette, G. R., Epstein, A. H., and Saxer, A. P., "The Influence of Inlet Temperature Distortion on Rotor Heat Transfer in a Transonic Turbine," AIAA Paper 95-3042, 1995.
[22] Harasgama, S. P., "Combustor Exit Temperature Distortion Effects on Heat Transfer and Aerodynamics within a Rotating Turbine Blade Passage," American Society of Mechanical Engineers Paper 90-GT-174, 1990.
[23] Gundy-Burlet, K. L., and Dorney, D. J., "Influence of 3D Hot Streaks on Turbine Heat Transfer," *International Journal of Turbo and Jet Engines*, Vol. 14, No. 3, 1997, pp. 123–132.
[24] Castillon, L., Laroche, E., and Sgarzi, O., "Unsteady Three-Dimensional Navier–Stokes Analysis of a Hot Streak Transport Through an Axial High Pressure Turbine Stage," International Symposium on Air Breathing Engines Paper 2003-1063, 2003.
[25] Fine Turbo User Manual 6-2-9, NUMECA International, Brussels, 2005.
[26] Arnone, A., and Pacciani, R., "Rotor-Stator Interaction Analysis Using the Navier–Stokes Equations and a Multigrid Method," *Journal of Turbomachinery*, Vol. 118, No. 3, 1996, pp. 679–689. doi:10.1115/1.2840923
[27] Rai, M. M., "Three-Dimension Navier–Stokes Simulations of Turbine Rotor-Stator Interaction, Part I—Methodology," *Journal of Propulsion and Power*, Vol. 5, No. 3, 1989, pp. 305–311. doi:10.2514/3.23154
[28] Spalart, P., and Allmaras, S., "A One-Equation Turbulence Model for Aerodynamic Flows," AIAA Paper 92-0439, 1992.
[29] Dorney, D. J., Sondak, D. L., and Cizmas, P. G. A., "Effects of Hot Streak/Airfoil Ratio in a High-Subsonic Single-Stage Turbine," AIAA Paper 99-2384, 1999.

A. Prasad
*Associate Editor*